

Formulation and study of thermal-mechanical coupling for saturated porous media

X. Wang^a, J. Dong^b

^aCollege of Engineering and Science, Louisiana Tech University, Ruston, LA 71272, USA

^bADINA R & D, Inc., Watertown, MA 02472 USA

Abstract

A formulation for the thermo-poro-elasto-plastic coupling analysis is presented, in which the energy balance equation is re-derived based on the concept of free enthalpy. The corresponding finite element procedures are developed and implemented into the commercial software ADINA. A complete solution strategy is described. The poro_mechanical and thermal coupling is conducted based on the simultaneous solution scheme for the isothermal poro-elasto-plastic interaction and the conventional thermal analysis. The complete solution procedures can be employed to solve both transient static and dynamic problems. The one-dimension column consolidation scenario is effectively re-examined with the proposed solution procedures, with heat and pore pressure dissipated on the top of the column. Accurate and reliable results with temperature and pore pressure distributions at different time steps are provided.

Keywords: Thermal-poro-elastoplastic coupling; Large strains, Finite element, Solution procedures

1. Introduction

As a multidisciplinary research area, the simulation of fluid flow and heat transfer in deformable porous media has challenged many scientists, mathematicians and computer engineers with mathematical difficulties and the cost of undue computational expenses

and efforts. This type of problems involves the interaction between fluid flow and thermal effects in saturated elasto-plastic porous materials under large deformations. During last decades, much attention has been drawn to find reliable and efficient formulations and solution procedures [5], [9], [14], [16], [24], [25]. A thermodynamics theory for elastic saturated porous solids has been presented by Biot [5], [6]. He introduced a rather novel concept of ‘principle of virtual dissipation’. Coussy [8], [9] gave a general theory of saturated porous solids under finite deformation employing the total Lagrangian formulation for the solid skeleton. A coupled finite element model was presented by Lewis [14], in which a partitioned solution procedure is carried out after the time domain interaction to restore the symmetry of the coefficient. Master et al. [17] proposed a model for deforming fissured porous media, in which two different porosities are defined for the porous medium and the fissured network, respectively. Based on a one-dimensional consolidation scenario, Bai and Abousleiman [3] discussed the necessity for a full coupling and the possibility of decoupling and tried to provide practical framework for the thermo-poro-elasto-plastic coupling analyses.

As described above, extensive papers have been published. Generally, the formulations are derived by making hypotheses such as isothermal process, infinitesimal deformation or elastic constitutive description for solid skeletons. The large deformation theories are either based on the Total Lagrangian formulation or the Updated Lagrangian formulation of a Jaumann rate-type [15]. Unfortunately, a robust solution algorithm capable of handling the large scale complex coupling analyses are not developed well enough to be used for practical analysis of prototype engineering structures.

In this paper, based on the finite element procedure proposed for the analysis of fully coupled thermo-elasto-plastic response of solids [18], we present the formulation and the implementation of a complete fully coupled thermal-poro-elasto-plastic model. In this model, the solid skeleton can be defined using various elasto-plastic material descriptions. The model is implemented for small strain and large strain analyses, which include the material non-linear only, the Total Lagrangian and the Updated Lagrangian formulations. The model is established with three equations for energy, momentum and fluid mass balances, together with the reduced energy dissipation inequality following from the Clausius-Duhem inequality form of the second law. The energy balance equation is re-derived based on the concept of free enthalpy, which is consistent with the equation Simo and Miehe [20] has obtained by taking the plastic entropy as an independent variable. The Darcy's law is used to describe the fluid flow through the porous media. The Fourier's law is prescribed for the heat flux. In the mechanical part, as a constitutive equation, the work done by Eterovic & Bathe [11] and Kojic & Bathe [12] is followed for large strain analysis using the Updated Lagrangian formulation of Hencky total strain type, i.e. the stress integration is carried out with a multiplicative decomposition of the deformation gradient tensor. The Hencky strain, a true strain used by many engineers, is obtained by the spectral decomposition of the right Cauchy-Green deformation tensor. For the thermal-poro_mechanical interaction, the framework proposed by Pantuso et al. [18] is followed and extended to consider the interaction between the solid skeleton and the pore fluid. In the porous media formulation, the pore fluid is assumed incompressible or slightly compressible. As an independent variable, the pore pressure is related to the effective stress by way of the effective stress principle assuming that the cauchy stress

imposing on the solid skeleton is equal to the total stress acting on the solid-fluid mixture minus the hydrostatic pore pressure. The Lagrangian permeability matrix and the Kirchhoff pore pressure are defined for the Total Lagrangian formulation. It implies that any spatially isotropic fluid flow will turn to be anisotropic under the original configuration. In the local multiplicative decomposition based Updated Lagrangian formulation, the generalized Darcy's law is employed. It describes under current configuration the relationship between the relative motion of the fluid with respect to that of the solid skeleton and the Kirchhoff pore pressure, which is defined as the spatial pore pressure times the volumetric ratio, the Jacobian of deformation gradient.

After the spatial finite element discretization, for the coupled algebraic equation system, the time integration scheme plays a very important role in reliable, efficient solution procedure. In this research work, for the solid skeleton-pore fluid mixture, the implicit Euler backward integration scheme is applied for both the mass balance equation and the momentum equation for the transient static analysis. In the transient dynamic analysis, the Euler backward method is used for the mass balance equation, and the Newmark method is employed for the momentum equation. For both static and dynamic analysis, the simultaneous solution strategy called direct solution procedure is adopted: nodal displacements and nodal spatial pore pressure are achieved simultaneously for the poro_mechanical system. For the thermal-poro_mechanical system, the classical non-linear iterative solution procedure is employed to have the coupled problem partitioned into poro_mechanical and thermal sub-problems. The numerical examples show that this solution algorithm can provide reliable and fast convergent solutions with less iterations.

2. Governing Equations

Our goal in this section is to describe the local governing equations of thermo-poro-elasto-plasticity at large deformation. For the energy and mass balances, the solid and the fluid phases would be considered separately. For the momentum balance, the mixture of the solid and fluid is taken into account, which leads to the effective stress principle. It has been widely used in engineering practice.

2.1. Mass balance for the pore fluid

As shown in Fig. 1, the unit volume ${}^{t+\Delta t}d\Omega$ has a volume change $dv = \Delta t \nabla \bullet {}^{t+\Delta t} \mathbf{V}_s$ from time t to $t+\Delta t$. At time t , the fluid mass contained in the infinitesimal volume is ${}^t\phi {}^t\rho_f$. Here, ϕ and ρ_f denote void ratio of the porous material and density of the pore fluid, respectively. The divergence operator ∇ is defined with respect to original coordinate system. \mathbf{V}_s represents the velocity tensor of the solid skeleton. After deformation, ${}^{t+\Delta t}d\Omega$ contains fluid mass ${}^{t+\Delta t}\phi {}^{t+\Delta t}\rho_f$. Obviously, the volume change dv is occupied by the fluid mass $\Delta t \nabla \bullet {}^{t+\Delta t} \mathbf{V}_s {}^{t+\Delta t}\rho_f$. The fluid mass flowing through the element surfaces of the infinitesimal volume is $\Delta t \nabla \bullet ({}^{t+\Delta t} \mathbf{V}_f - {}^{t+\Delta t} \mathbf{V}_s) {}^{t+\Delta t}\rho_f$. The law of mass conservation implies that

$${}^{t+\Delta t}\phi {}^{t+\Delta t}\rho_f + \Delta t \nabla \bullet {}^{t+\Delta t} \mathbf{V}_s {}^{t+\Delta t}\rho_f + \Delta t \nabla \bullet ({}^{t+\Delta t} \mathbf{V}_f - {}^{t+\Delta t} \mathbf{V}_s) {}^{t+\Delta t}\rho_f = {}^t\phi {}^t\rho_f \quad (1)$$

It can be re-written using material time derivation in Lagrangian description with left superscripts omitted

$$\frac{d(\phi\rho_f)}{dt} + \nabla \bullet \mathbf{V}_s \rho_f + \nabla \bullet \tilde{\mathbf{V}} \rho_f = 0 \quad (2)$$

with $\tilde{\mathbf{V}} = \phi \mathbf{V}_r = \phi(\mathbf{V}_f - \mathbf{V}_s)$, in which the relative velocity \mathbf{V}_r is defined as the Darcy velocity. \mathbf{V}_f denotes the intrinsic fluid velocity. If the porous fluid is assumed slightly compressible, the fluid density might be considered constant. Then equation (2) can be simplified as

$$\frac{d\phi}{dt} + \nabla \cdot \mathbf{V}_s + \nabla \cdot \tilde{\mathbf{V}} = 0 \quad (3)$$

which is consistent with the equation Desai and Christian presented [10]. Equation (3) will be used in the implementation of the finite element formulation. With the assumption of incompressible solid particles, the current void ratio can be obtained based on the original void ratio ${}^0\phi$ and the current volume ratio ${}^{t+\Delta t}J$

$${}^{t+\Delta t}\phi = 1 - (1 - {}^0\phi) {}^{t+\Delta t}J^{-1} \quad (4)$$

Served as the constitutive model for pore fluid flow, the generalized Darcy's law reads [9]

$$\tilde{\mathbf{V}} = -\mathbf{K} \cdot (\nabla p^f) - \mathbf{K} \cdot \mathbf{C}_{FT} \cdot (\mathbf{q} / \theta) \quad (5)$$

where \mathbf{K} is the second-order current permeability tensor, p^f is the total pore pressure. θ is the current absolute temperature, \mathbf{q} is referred to as the heat flow and \mathbf{C}_{FT} denotes a parameter tensor associated with the fluid mass and thermal flows. The second term on the right side of equation (5) is herein ignored, which was justified by Advani [2] and Lewis [14]. Substituting equation (5) to equation (3), we obtain

$$\frac{d\phi}{dt} + \nabla \cdot \mathbf{V}_s + \nabla^T \cdot (-\mathbf{K} \cdot (\nabla p^f)) = 0 \quad (6)$$

The volumetric change of the slight compressible fluid can be computed using the Hook's law. Then

$$\frac{d\phi}{dt} = \phi \left(\frac{1}{K_f} \frac{\partial p^f}{\partial t} + \beta_f \frac{\partial \theta}{\partial t} \right) \quad (7)$$

where K_f is the compressibility of the fluid, β_f is the thermal expansion parameter of the fluid. Incorporating equation (7) into (6) and expressing $\nabla \bullet \mathbf{V}_s$ with volumetric strain rate plus thermal expansion of the solid skeleton, the following equation is obtained

$$\varphi \frac{1}{K_f} \frac{\partial p^f}{\partial t} + \frac{\partial \varepsilon_{ii}}{\partial t} + (1 - \varphi) \beta_s \frac{\partial \theta}{\partial t} + \varphi \beta_f \frac{\partial \theta}{\partial t} + \nabla^T \bullet (-\mathbf{K} \bullet (\nabla p^f)) = 0 \quad (8)$$

in which β_s is the thermal expansion coefficient for the solid skeleton.

2.2 Momentum balance of the saturated solid skeleton and fluid mixture

As in the iso-thermal case, the pore fluid acts as ‘perfect fluid’ [22], and has no capability to resist shear and traction. The pore pressure does not cause solid particles to be pressed together. The effective stress principle in current configuration with true stresses is re-written as

$$\sigma_{ij} = \tilde{\sigma}_{ij} + p^f \delta_{ij} \quad (i, j = 1, 2, 3) \quad (9)$$

where σ_{ij} denote the total cauchy stress components, $\tilde{\sigma}_{ij}$ are the cauchy effective stresses, and p^f is the cauchy pore pressure, and δ_{ij} is the Kronecker-Delta. It takes the following form in the original configuration.

$$\mathbf{S}_{ij} = \tilde{\mathbf{S}}_{ij} + P^f \mathbf{C}^{-1} \delta_{ij} \quad (10)$$

where \mathbf{S} represents the second Piola-Kirchhoff stress tensor, \mathbf{C} is the right Cauchy-Green deformation tensor, and given by $\mathbf{C} = \mathbf{X}^T \mathbf{X}$. \mathbf{X} signifies the deformation gradient tensor. P^f is called the Kirchhoff pore pressure [7], which is equal to the cauchy pore pressure multiplied by the volumetric ratio J . From equation (10), we know that $P^f \mathbf{C}^{-1}$ acts no longer equally in every direction if it is viewed as the second Piola-Kirchhoff pore pressure. The local equations of motion are expressed here for the numerical

implementation of the finite element algorithm [20]. Considering the effective stress principle, the linear momentum equation in current configuration, is taken as

$${}^{t+\Delta t} \tilde{\sigma}_{ij,j} + {}^{t+\Delta t} P_{ij}^f \delta_{ij} + {}^{t+\Delta t} \rho {}^{t+\Delta t} b_i = {}^{t+\Delta t} \rho {}^{t+\Delta t} \ddot{x}_i \quad (i, j=1, 2, 3) \quad (11)$$

where j implies the first derivative with respect to the current configuration, ${}^{t+\Delta t} \rho$ is the current density of the solid-fluid mixture, ${}^{t+\Delta t} b_i$ is the current body force and ${}^{t+\Delta t} \ddot{x}_i$ is the current acceleration. In the original configuration, the momentum equation becomes

$${}^{t+\Delta t} \tilde{P}_{ij,j} + {}^{t+\Delta t} P_{ij,j}^f \delta_{ij} + {}^0 \rho {}^0 B_i = {}^0 \rho {}^{t+\Delta t} \ddot{x}_i \quad (12)$$

\tilde{P}_{ij} is the non-symmetric nominal stress tensor. It is written as

$${}^{t+\Delta t} \tilde{P}_{ij} = {}^{t+\Delta t} X_{im} {}^{t+\Delta t} S_{mj} \quad (m=1, 2, 3) \quad (13)$$

Here, ${}^0 \rho$ is the corresponding density in the original configuration, ${}^0 B_i$ is the body force, and ${}^{t+\Delta t} P_{ij}^f$, the first Piola-Kirchhoff pore pressure, is expressed by

$${}^{t+\Delta t} P_{ij,j}^f = {}^{t+\Delta t} J {}^{t+\Delta t} P_{ij}^f \left({}^{t+\Delta t} X_{ij} \right)^{-T} \quad (14)$$

2.3 Thermomechanics of saturated porous media

Expressed in the special case of the Clausius-Plank form, the second law, the principle of dissipation, can be written as [23]

$$\Omega = \theta \gamma_{loc} = \boldsymbol{\tau} : \mathbf{d} + \theta \dot{\eta} - \dot{v} \geq 0 \quad (15)$$

In the above-mentioned energy dissipation inequality, $\boldsymbol{\tau}$ are the Cauchy stresses, \mathbf{d} are the rates of the deformation tensor. γ_{loc} is referred to as the local entropy production, η denotes the total entropy, θ is the absolute temperature, and v is the specific internal energy.

In addition to the linear momentum and continuity equation described in the last subsection, the thermomechanical response of the porous media is also governed by the energy balance equation, which is described as the first law of thermodynamics.

$$\dot{w} - \dot{w} = -\text{Jdiv}(q) + r \quad (16)$$

In this relation, w is the specific mechanical work, q denotes the heat flux and r denotes the specific heat source. $\text{div}(\bullet)$ represents the divergence in the current configuration.

The mechanical work rate can be decomposed into two parts: reversible part \dot{w}_r and remaining part \dot{w}_i . The remaining part can be split into the other two parts: the dissipated part \dot{w}_d and the part \dot{w}_h leading to changes in the stored energy [13], i.e.

$$\dot{w} = \dot{w}_r + \dot{w}_h + \dot{w}_d \quad (17)$$

In equation 16, the internal energy can be specified as

$$v = \hat{v}(\mathbf{C}^e, \boldsymbol{\tau}, \theta, \eta) \quad (18)$$

where $\mathbf{C}^e = (\mathbf{X}^e)^T \mathbf{X}^e$ denotes the elastic right cauchy-green deformation tensor. The specific free enthalpy function $\hat{\psi}$ is achieved by a double Legendre transformation [13].

$$\hat{\psi} = v - \boldsymbol{\tau} \cdot \boldsymbol{\varepsilon}^e - \theta \eta \quad (19)$$

The evolution of the specific free enthalpy $\dot{\psi} = \dot{\psi}(\boldsymbol{\tau}, \Gamma, \theta)$ is expressed as

$$\dot{\psi} = \dot{v} - \dot{\boldsymbol{\varepsilon}}^e \cdot \boldsymbol{\tau} - \dot{\theta} \eta - \theta \dot{\eta} \quad (20)$$

Substituting equation (17) into (16) then taking (16) to (20), and noting $\dot{w}_r = \boldsymbol{\tau} \cdot \dot{\boldsymbol{\varepsilon}}$, we

have

$$\dot{w} = \dot{w}_h + \dot{w}_d - \dot{\boldsymbol{\varepsilon}}^e \cdot \boldsymbol{\tau} - \text{div}(q) + r - \dot{\theta} \eta - \theta \dot{\eta} \quad (21)$$

On the other hand, we take time derivation of ψ , and express the thermic state and caloric state equations, respectively as follows [13]

$$\mathcal{E} = -\frac{\partial \hat{\psi}}{\partial \tau} \text{ and } \eta = -\frac{\partial \hat{\psi}}{\partial \theta} \quad (22)$$

and make it equal to (21). Gibb's equation is obtained eventually

$$\theta \dot{\mathcal{E}} = \dot{\mathcal{W}}_h + \dot{\mathcal{W}}_d - \text{div}(\mathbf{q}) + r - \frac{\partial \hat{\psi}}{\partial \Gamma} \dot{\Gamma} \quad (23)$$

Where Γ stand for a set of internal variables. The mechanical work rate $\dot{\mathcal{W}}_h$ in changing the internal structure of the material is balanced by the non-dissipated part $\frac{\partial \hat{\psi}}{\partial \Gamma} \dot{\Gamma}$.

Therefore, the Gibb's equation is re-written as

$$\theta \dot{\mathcal{E}} = \dot{\mathcal{W}}_d - \text{div}(\mathbf{q}) + r \quad (24)$$

Alternatively, time derivation of the entropy η expressed in (22) gives

$$\dot{\eta} = -\left(\frac{\partial^2 \hat{\psi}}{\partial^2 \theta} \dot{\theta} + \frac{\partial \hat{\psi}}{\partial \theta} \dot{\theta} \right) \quad (25)$$

Since \mathbf{C}^e is conjugate with τ , the evolution of the free enthalpy function is also expressed as

$$\dot{\mathcal{E}} = \frac{\partial \hat{\psi}}{\partial \theta} \dot{\theta} + \frac{\partial \hat{\psi}}{\partial \mathbf{C}^e} \dot{\mathbf{C}}^e + \frac{\partial \hat{\psi}}{\partial \Gamma} \dot{\Gamma} \quad (26)$$

Substituting equations (26) into (25), and taking (25) into (23), we obtain finally

$$-\theta \frac{\partial^2 \hat{\psi}}{\partial^2 \theta} \dot{\theta} - \theta \left(\frac{\partial^2 \hat{\psi}}{\partial \mathbf{C}^e \partial \theta} \dot{\mathbf{C}}^e + \frac{\partial^2 \hat{\psi}}{\partial \Gamma \partial \theta} \dot{\Gamma} \right) = \dot{\mathcal{W}}_d - \text{div}(\mathbf{q}) + r \quad (27)$$

$\dot{\mathcal{W}}_d$ is called the plastic heat, generated from the dissipation part of the plastic work, which is expressed by Lehmann [13] as

$$\mathbf{w}_{\mathcal{d}} = (1 - \xi) \boldsymbol{\tau} \cdot \mathcal{E} \quad (28)$$

ξ is looked upon as a material parameter. Finally, the energy balance equation reads

$$C_{\theta} \dot{\mathcal{E}} = (1 - \xi) \boldsymbol{\tau} \cdot \mathcal{E} - H - \text{div}(\mathbf{q}) + \mathbf{r} \quad (29)$$

$$C_{\theta} = -\theta \frac{\partial^2 \hat{\psi}}{\partial^2 \theta}, \quad H = -\theta \left(\frac{\partial^2 \hat{\psi}}{\partial \mathbf{C}^e \partial \theta} \mathbf{C}^e + \frac{\partial^2 \hat{\psi}}{\partial \Gamma \partial \theta} \mathbf{F} \right) \quad (30)$$

where C_{θ} , a material constant, represents the specific heat capacity, H is called non-dissipative elastic-plastic heating. Because of the definitions of the free enthalpy and free energy functions and their uncoupled components, C_{θ} and H can be re-written in terms of free energy function φ as

$$C_{\theta} = -\theta \frac{\partial^2 \varphi}{\partial^2 \theta}, \quad H = -\theta \left(\frac{\partial^2 \varphi}{\partial \mathbf{C}^e \partial \theta} \mathbf{C}^e + \frac{\partial^2 \varphi}{\partial \Gamma \partial \theta} \mathbf{F} \right) \quad (31)$$

Comparing equation (29) with the similar result given by Simo and Miehe [21], the mechanical dissipation Q_{mech} , not completely dissipated as plastic heat, includes a part of the energy, which is stored for the change of the internal structure. Please note that the plastic entropy η^p is not assumed a state variable in deriving equation (29) as done by Simo and Miehe.

For saturated porous material, the energy balance equation is written as by referring to Lewis and others [14]

$$\left[(1 - \phi)^t \theta \frac{\partial^2 \varphi_s}{\partial^2 \theta} - \phi^t \theta \frac{\partial^2 \varphi_f}{\partial^2 \theta} \right] \dot{\mathcal{E}} = \text{div}(\mathbf{q}) - H + (1 - \xi) \boldsymbol{\tau} \cdot \mathcal{E} + \mathbf{r} \quad (32)$$

H is related to the non-dissipative elasto-plastic structural changes. It is ignored by many researchers (Pantuso et al. [18]; Lewis et al. [14]; Shanghvi and Michalevis [19]). H is also omitted in the implementation of the algorithm proposed in the paper.

2.4 Boundary conditions

For the solution of thermomechanical porous media problem, the following boundary condition must be specified.

1) Essential boundaries

Prescribed displacement on boundary V_u^E is

$$\mathbf{u} = \mathbf{u}^b \text{ on } \partial^0 V_u^E; \quad (33)$$

and/or temperature boundary is specified by

$$\theta = \theta^b \text{ on } \partial^0 V_\theta^E; \quad (34)$$

In many cases, pore pressure boundaries need to be prescribed as

$$p = p^b \text{ on } \partial^0 V_p^E; \quad (35)$$

2) Natural boundaries

The pressure boundary for mechanical part is written as

$$\mathbf{S} \bullet \mathbf{n} |_{\partial^0 V_s^N} = S_n \quad (36)$$

Where S_n is the total pressure on the corresponding boundary. Heat flux condition for the thermal part is given by

$$k_n^h \frac{\partial \theta}{\partial \mathbf{n}} |_{\partial^0 V_{qh}^N} = q_h^s \quad (37)$$

where k_n^h is the component of the thermal conductivity tensor in the normal direction of the boundary.

For the pore fluid part, fluid flux boundary is given as

$$k_n^f \frac{\partial p}{\partial \mathbf{n}} |_{\partial^0 V_{qf}^N} = q_f^s \quad (38)$$

where k_n^f denotes the body permeability tensor in normal direction of the porous boundary.

The whole body boundary can be expressed as

$$\partial^0 \mathbf{V} = \partial^0 \mathbf{V}_u^E \cup \partial^0 \mathbf{V}_s^N = \partial^0 \mathbf{V}_\theta^E \cup \partial^0 \mathbf{V}_{q_h}^N = \partial^0 \mathbf{V}_p^E \cup \partial^0 \mathbf{V}_{q_f}^N \quad (39)$$

and

$$\partial^0 \mathbf{V}_u^E \cap \partial^0 \mathbf{V}_s^N = \partial^0 \mathbf{V}_\theta^E \cap \partial^0 \mathbf{V}_{q_h}^N = \partial^0 \mathbf{V}_p^E \cap \partial^0 \mathbf{V}_{q_f}^N = \mathbf{0} \quad (40)$$

3. The finite element equations for the thermal-poro_mechanical coupling of the saturated porous media

With the rules for the standard finite element discretization [2] applied to the governing equations (8), (11) and (29), the finite element equations can be formed in the following coupled systems of coupled equations. For the iso-thermal porous structure in transient static state,

$$\begin{bmatrix} \underline{\mathbf{0}} & \underline{\mathbf{0}} \\ {}^{t+\Delta t} \mathbf{K}_{up_f}^T & {}^{t+\Delta t} \mathbf{K}_{p_f p_f}^{(1)} \end{bmatrix} \begin{bmatrix} {}^{t+\Delta t} \underline{\dot{\mathbf{U}}} \\ {}^{t+\Delta t} \underline{\dot{\mathbf{P}}}_f \end{bmatrix} + \begin{bmatrix} {}^{t+\Delta t} \mathbf{K}_{uu} & {}^{t+\Delta t} \mathbf{K}_{up_f} \\ \underline{\mathbf{0}} & -{}^{t+\Delta t} \mathbf{K}_{p_f p_f}^{(2)} \end{bmatrix} \begin{bmatrix} {}^{t+\Delta t} \underline{\mathbf{U}} \\ {}^{t+\Delta t} \underline{\mathbf{P}}_f \end{bmatrix} = \begin{bmatrix} {}^{t+\Delta t} \underline{\mathbf{R}}_u \\ {}^{t+\Delta t} \underline{\mathbf{R}}_{p_f} \end{bmatrix} = [{}^{t+\Delta t} \underline{\mathbf{R}}_{fs}] \quad (41)$$

Where ${}^{t+\Delta t} \underline{\mathbf{U}}$ and ${}^{t+\Delta t} \underline{\mathbf{P}}_f$ are nodal displacement and pore pressure variables, respectively.

This equation group can apply to the cases of small and large strains. Similar results were given by Simon et al. [22]. For the transient dynamic state, the governing equations are

$$\begin{aligned}
& \begin{bmatrix} {}^{t+\Delta t} \mathbf{M} & \underline{\mathbf{0}} \\ \underline{\mathbf{0}} & \underline{\mathbf{0}} \end{bmatrix} \begin{bmatrix} {}^{t+\Delta t} \ddot{\underline{\mathbf{U}}} \\ {}^{t+\Delta t} \ddot{\underline{\mathbf{P}}}_f \end{bmatrix} + \begin{bmatrix} {}^{t+\Delta t} \underline{\mathbf{C}} & \underline{\mathbf{0}} \\ {}^{t+\Delta t} \mathbf{K}_{up_f}^T & {}^{t+\Delta t} \mathbf{K}_{p_f p_f}^{(1)} \end{bmatrix} \begin{bmatrix} {}^{t+\Delta t} \dot{\underline{\mathbf{U}}} \\ {}^{t+\Delta t} \dot{\underline{\mathbf{P}}}_f \end{bmatrix} + \\
& \begin{bmatrix} {}^{t+\Delta t} \mathbf{K}_{uu} & {}^{t+\Delta t} \mathbf{K}_{up_f} \\ \underline{\mathbf{0}} & -{}^{t+\Delta t} \mathbf{K}_{p_f p_f}^{(2)} \end{bmatrix} \begin{bmatrix} {}^{t+\Delta t} \underline{\mathbf{U}} \\ {}^{t+\Delta t} \underline{\mathbf{P}}_f \end{bmatrix} = \begin{bmatrix} {}^{t+\Delta t} \underline{\mathbf{R}}_u \\ {}^{t+\Delta t} \underline{\mathbf{R}}_{p_f} \end{bmatrix} = \begin{bmatrix} {}^{t+\Delta t} \mathbf{R}_{fs} \end{bmatrix} \quad (41)
\end{aligned}$$

Where the stiffness matrix components are given by

$${}^{t+\Delta t} \mathbf{K}_{uu} = \sum_m \int_{t+\Delta t V^{(m)}} {}^{t+\Delta t} \mathbf{B}_u^{(m)T} {}^{t+\Delta t} \mathbf{C}_{ep}^{(m)} {}^{t+\Delta t} \mathbf{B}_u^{(m)} d^{t+\Delta t} V^{(m)}$$

$${}^{t+\Delta t} \mathbf{K}_{up_f} = \sum_m \int_{t+\Delta t V^{(m)}} {}^{t+\Delta t} \mathbf{B}_u^{(m)T} \mathbf{I}^{(m)} {}^{t+\Delta t} \mathbf{H}_{p_f}^{(m)} d^{t+\Delta t} V^{(m)}$$

$${}^{t+\Delta t} \mathbf{K}_{p_f p_f}^{(1)} = \frac{1}{K_f} \sum_m \int_{t+\Delta t V^{(m)}} {}^{t+\Delta t} \varphi^{(m)} {}^{t+\Delta t} \mathbf{H}_{p_f}^{(m)T} {}^{t+\Delta t} \mathbf{H}_{p_f}^{(m)} d^{t+\Delta t} V^{(m)}$$

$${}^{t+\Delta t} \mathbf{K}_{p_f p_f}^{(2)} = \sum_m \int_{t+\Delta t V^{(m)}} {}^{t+\Delta t} \mathbf{B}_{p_f}^{(m)T} {}^{t+\Delta t} \mathbf{k}^{(m)} {}^{t+\Delta t} \mathbf{B}_{p_f}^{(m)} d^{t+\Delta t} V^{(m)}$$

$${}^{t+\Delta t} \mathbf{R}_u = \sum_m \int_{t+\Delta t V^{(m)}} {}^{t+\Delta t} \mathbf{H}_u^{(m)T} {}^{t+\Delta t} \mathbf{f}^{(m)} d^{t+\Delta t} V^{(m)} + \sum_m \int_{t+\Delta t V^{(m)}} {}^{t+\Delta t} \beta^{t+\Delta t} \mathbf{H}_u^{(m)T} \Delta \theta d^{t+\Delta t} V^{(m)} +$$

$$\sum_m \int_{t+\Delta t S_f^m} {}^{t+\Delta t} \mathbf{H}_u^{t+\Delta t S_f^m} {}^{t+\Delta t} \mathbf{f}^{(m)} d^{t+\Delta t} S_f^{(m)}$$

$${}^{t+\Delta t} \mathbf{R}_{p_f} = \sum_m \int_{t+\Delta t S_q^{(m)}} {}^{t+\Delta t} \mathbf{H}_{p_f}^{t+\Delta t S_q^{(m)}} {}^{t+\Delta t} \mathbf{q}_f^{(m)} d^{t+\Delta t} S_q^{(m)}$$

where $\underline{\mathbf{C}}$ and \mathbf{M} denote, respectively, damping matrix and mass matrix of the finite element assemblage under the current configuration. \mathbf{C}_{ep} is the elasto-plastic constitutive matrix. \mathbf{f} and \mathbf{q} denote load vectors (force, traction and fluid flux, etc.). \mathbf{B}_u , \mathbf{B}_{p_f} are gradient matrices for the displacements $\underline{\mathbf{U}}$ and pore pressure $\underline{\mathbf{P}}_f$, respectively. \mathbf{H}_u and \mathbf{H}_{p_f} are interpolation matrices, respectively for the displacements $\underline{\mathbf{U}}$ and pore

pressure $\underline{\mathbf{P}}_f$. \mathbf{I} is the identity tensor. β , the synthetic thermal expansion coefficient, is void ratio-based weighed as given in equation (44).

For the thermal part, the discretized finite element equations are

$$\begin{aligned}
& \left(\sum_m \int_{t+\Delta t V^{(m)}} {}^{t+\Delta t} \mathbf{H}_\theta^{(m)T} {}^{t+\Delta t} \mathbf{C}_\theta d {}^{t+\Delta t} \mathbf{V}^{(m)} \right) {}^{t+\Delta t} \boldsymbol{\theta} + \left(\sum_m \int_{t+\Delta t V^{(m)}} {}^{t+\Delta t} \mathbf{B}_\theta^T {}^{t+\Delta t} \mathbf{k}_\theta {}^{t+\Delta t} \mathbf{B}_\theta d {}^{t+\Delta t} \mathbf{V}^{(m)} \right) {}^{t+\Delta t} \boldsymbol{\theta} \\
& = \sum_m \int_{t+\Delta t V^{(m)}} {}^{t+\Delta t} \mathbf{H}_\theta^{(m)T} {}^{t+\Delta t} \mathbf{Q}_M^{(m)} d {}^{t+\Delta t} \mathbf{V}^{(m)} + \sum_m \int_{t+\Delta t V^{(m)}} {}^{t+\Delta t} \mathbf{H}_\theta^{(m)T} {}^{t+\Delta t} \mathbf{q}_\theta^{(m)} d {}^{t+\Delta t} \mathbf{V}^{(m)} + \\
& \sum_m \int_{\partial^{t+\Delta t} S_q^{(m)}} {}^{t+\Delta t} \mathbf{H}_\theta^{(s)T} {}^{t+\Delta t} \mathbf{q}_\theta^{(s)} d {}^{t+\Delta t} \mathbf{S}_q^{(m)} \\
& = {}^{t+\Delta t} \mathbf{R}_{th}
\end{aligned} \tag{42}$$

where \mathbf{C}_θ is the material constant tensor, called the specific heat capacity, as expressed in equation (30). \mathbf{k}_θ , another material property tensor, denotes the thermal conductivity.

\mathbf{Q}_M is equivalent to the \mathbf{w}_q , given in equation (28), is rewritten as [1]

$$\mathbf{Q}_M = \omega \boldsymbol{\tau} \cdot \mathbf{D}^p \tag{43}$$

in which $\boldsymbol{\tau}$ is the cauchy stress tensor at current configuration, \mathbf{D}^p is the plastic strain rate tensor, and ω represents a material parameter. \mathbf{B}_θ is a gradient matrix for nodal temperature θ , \mathbf{H}_θ is the temperature interpolation function.

4. Solution strategy

A conceptual solution procedure is given in this section, which is based on the foregoing presented algorithm. The Newton's method with line search scheme is a very efficient way to apply for the coupled thermo-poro_mechanical equations. The closest point return mapping methods based on implicit backward stress integration algorithms are

used for various nonlinear and elastic-plastic material models. The thermo-poro_mechanical coupling system is decomposed as two sub-coupling systems. One is the coupling between the pore-fluid and the porous structure it flows through. A simultaneous solution is employed for this coupled system of equations, i.e., solutions for fluid variables like pore pressure and mechanical variables such as stresses, displacements and other internal variables are obtained simultaneously at each iteration. The computation is conducted with one poro_mechanical finite element code. The other one is the thermal and poro_mechanical coupling, which is implemented with one independent mechanical code and one thermal finite element code, with temperature- and stress-dependent mechanical and fluid parameters and stress-dependent thermal parameters introduced in the mechanical code if necessary. The heat flux generated by the plastic straining is also computed in the mechanical code, as described by Pantuso et al. [18]. In the following computational procedure, the solutions are assumingly completed at time step t , and solution time is $t + \Delta t$.

- 1) **Initial data available at t .** converged solutions have been obtained at time step t .
 - a. Displacement ${}^t\mathbf{d}$ and pore pressure ${}^t\mathbf{p}$ at nodal points, strains, stresses and internal variables ${}^t\boldsymbol{\varepsilon}$, ${}^t\boldsymbol{\sigma}$, ${}^t\boldsymbol{\gamma}$, etc. on Gauss points of each element for the mechanical code.
 - b. Temperature ${}^t\boldsymbol{\theta}$ on nodal points for the thermal code.
 - c. Calculation of the initial stiffness matrix and forcing vector ${}^{t+\Delta t}\mathbf{R}_{fs}$, as shown in equation (40) or (41) for the solid-fluid system.
- 2) **Poro_Mechanical analysis.** At the fixed initial temperature ${}^t\boldsymbol{\theta}$, perform the coupled-simultaneous computation for the pore-fluid and structure system at time step $t + \Delta t$.

- a. Compute ${}^{t+\Delta t} \mathbf{d}$ and ${}^{t+\Delta t} \mathbf{p}$ based on the initial stiffness matrix and force vector ${}^{t+\Delta t} \mathbf{R}_{fs}$.
- b. Perform return mapping method to take stress integration at each Gauss point to get stresses, strains, plastic heat and some other internal variables.
- c. Calculate residuals for the force vector ${}^{t+\Delta t} \mathbf{R}_{fs}$, displacement vector ${}^{t+\Delta t} \mathbf{d}$, pore pressure vector ${}^{t+\Delta t} \mathbf{p}$ and strain energy ${}^{t+\Delta t} E$. If all of the employed convergence criteria are not satisfied, update stresses, strains, plastic heat, some other internal variables and consistent tangential constitutive matrix, then go to step 2(a). If the criteria are satisfied go to step 3.

3) **Thermal analysis.** Perform thermal analysis with fixed configuration and fluid state at ${}^{t+\Delta t} \mathbf{d}$ and ${}^{t+\Delta t} \mathbf{p}$, which have been obtained at step 2(c). Thermal loading and thermal boundary conditions are updated to current time step $t + \Delta t$. New solution ${}^{t+\Delta t} \boldsymbol{\theta}$ is obtained at element nodal points by solving equation (42) using the same mesh or different mesh for the mechanical-pore fluid coupling analysis. In the thermal analysis, a one-phase material will approximately replace the two-phase mixture. For the one-phase material, the void-ratio based weighed thermal parameters and densities are specified by

$$\begin{cases} {}^{t+\Delta t} C_{\theta} = (1 - \phi) {}^{t+\Delta t} C_{\theta}^{\text{solid}} + \phi {}^{t+\Delta t} C_{\theta}^{\text{fluid}} \\ {}^{t+\Delta t} \mathbf{k}_{\theta} = (1 - \phi) {}^{t+\Delta t} \mathbf{k}_{\theta}^{\text{solid}} + \phi {}^{t+\Delta t} \mathbf{k}_{\theta}^{\text{fluid}} \\ {}^{t+\Delta t} \rho_{\theta} = (1 - \phi) {}^{t+\Delta t} \rho_{\theta}^{\text{solid}} + \phi {}^{t+\Delta t} \rho_{\theta}^{\text{fluid}} \\ {}^{t+\Delta t} \beta_{\theta} = (1 - \phi) {}^{t+\Delta t} \beta_{\theta}^{\text{solid}} + \phi {}^{t+\Delta t} \beta_{\theta}^{\text{fluid}} \end{cases} \quad (44)$$

4) **Thermal-Poro_Mechanical interaction.** The poro_mechanical analysis is performed again with new temperature solution ${}^{t+\Delta t} \boldsymbol{\theta}$. Compute poro_mechanical residual ${}^{t+\Delta t} \mathbf{R}_{fs}$ for each element contribution. If ${}^{t+\Delta t} \mathbf{R}_{fs}$ is within the tolerance, the iteration

terminates. Otherwise, the iteration proceeds until $\left|{}^{t+\Delta t} \mathbf{R}_{fs}\right| < \text{TOL1}$. Displacement ${}^{t+\Delta t} \mathbf{d}$, pore pressure ${}^{t+\Delta t} \mathbf{p}$, plastic heat ${}^{t+\Delta t} \mathbf{Q}_M$ and internal variables ${}^{t+\Delta t} \mathbf{\Gamma}$ are thereafter updated. Similarly, thermal residual ${}^{t+\Delta t} \mathbf{R}_{th}$ represented by the sum of terms at the right side of equation (42), contributed by each element, are calculated with the updated plastic heat ${}^{t+\Delta t} \mathbf{Q}_M$. The thermal analysis is performed again unless $\left|{}^{t+\Delta t} \mathbf{R}_{fth}\right| < \text{TOL2}$. Similar iteration loop is circulated for both poro_mechanical and Thermal analyses until all the specified convergence criteria are satisfied.

5. The porous column consolidation along with its temperature dissipation---a numerical example

The fluid-saturated column, as schemed in figure 2(a), is viewed as a 2-D axisymmetrical problem. As a straightforward example, it is re-examined with the proposed formulation in this paper for the saturated porous media under the circumstance of temperature dissipation. The porous column with the porosity equal to 0.25, 100m long and 6m wide, is confined on, and impermeable through lateral and bottom surfaces, which also insulate heat conduction. An initial uniform temperature of 10°C applies to the column, but its top is set to 0°C to induce transient heat conduction through the column. A pressure of 500 kPa is exerted on the top of the column before pore pressure and heat dissipate from the top. In order to make an undrained condition, the pore pressure is set to start to dissipate from the top boundary 5 hours after the temperature does. The column is discretized with 20 4-node solid elements (figure 2(b)), and the mechanical, thermal, and hydraulic parameters are listed in tables 1, 2 and 3, respectively.

Table 1 Mechanical parameters

| Temperature (°C) | Young's modulus (KPa) | Poisson's ratio | Yield stress (KPa) | Strain hardening modulus (KPa) | Thermal expansion coefficient (°C ⁻¹) | |
|---------------------|-----------------------------|--------------------|-----------------------|---|---|---------|
| | | | | | Solid | Fluid |
| -1000.0 | 2.0E5 | 0.3 | 280.4 | 270 | 2.66E-6 | 40.0E-6 |
| 1000.0 | 2.0E5 | 0.3 | 100.4 | 270 | 2.66E-6 | 40.0E-6 |

Table 2 Thermal properties

| Temperature (°C) | Conductivity (J/m,h,°C) | | Heat capacity (J/kg,°C) | |
|---------------------|-------------------------|-------|-------------------------|-------|
| | Solid | Fluid | Solid | Fluid |
| -10000.0 | 26.67 | 100 | 35.88 | 35.88 |
| 10000.0 | 50 | 35 | 35.88 | 35.88 |

Table 3 Hydraulic parameters

| Temperature (°C) | Permeability | Permeability | Porosity |
|------------------|---------------------------------------|---------------------------------------|----------|
| | K _x (m ³ .h/kg) | K _y (m ³ .h/kg) | |
| -10000.0 | 1.0e-7 | 1.0e-7 | 0.25 |
| 10000.0 | 1.0e-7 | 1.0e-7 | 0.25 |

Within the first 5 hours, pore fluid does not dissipate out of the structure, which is under the undrained condition. However, the pore pressure at the bottom does not reach the maximum value—500 KPa due to the existence of thermal strain. Because of the dissipation of the temperature, the pore pressure near the end of the column shows the Mandel effect: It even rises slightly before it drops at the early stage of the consolidation. With the dissipation of pore pressure and temperature, the effective stress will progressively increase and exceed the yield stress from the top to bottom. Plastic zone

will initiate at the top of the column, and gradually propagate down to lower part of the column. The transient deformation, affected by the transient temperature and pore pressure, eventually turns the whole column into a plastic zone. The dissipations of pore pressure and temperature at the bottom of the porous column are shown in figures 3 and 9, respectively. Another set of pore pressure and temperature dissipation results at the same place are also displayed in figures 4 and 10, respectively, which are achieved without considering the thermal-poro_mechanical coupling. Those solutions show that the initial temperature has slowed down the dissipation of the pore pressure. On the other hand, the rate of temperature dissipation has also been reduced if considering the generation of the plastic heat by conducting the thermal-poro_mechanical coupling analysis. The reduction of consolidation rate can also be discerned from the settlement solutions (figures 5 and 6), and the changes in effective stress at the bottom of the column (figures 7 and 8).

6. Conclusions

The formulation for thermal-poro-elasto-plastic coupling is introduced. It is worthwhile to note that the energy balance equation is re-derived in this paper based on the concept of free enthalpy, which is consistent with the equation obtained by Simo and Miche [20] with the explicit introduction of plastic entropy as an independent variable. The formulation is implemented into ADINA with implicit stress integration algorithms for small and large strain cases. It can be employed for both transient static and dynamic analysis. The isothermal fluid-solid coupling (poro_mechanical coupling) is carried out as an independent portion, and simultaneous results are given. Thermal analysis on a

fixed structural configuration is conducted separately. The solution procedures for the thermal-poro_mechanical coupling are described in details. As a simple example, the porous column consolidation problem is re-examined using the proposed numerical framework, in which an initial temperature is assumed for the whole area, and temperature and pore pressure dissipations occur on the top of column. Pore pressure, temperature, effective stress and displacement solutions are obtained at different time steps, which are proved reasonable and accurate.

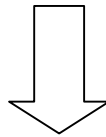
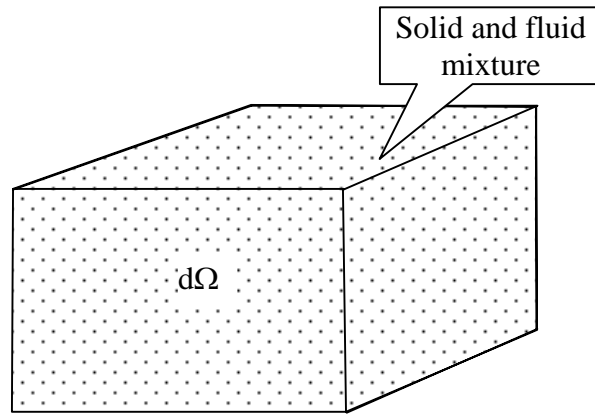
References

- [1] ADINA R & D, Inc. Theory and Modelling Guide 2001. Vol. II: ADINA-T: 75-77.
- [2] Advani SH, Lee TS, Lee JK, Kim CS. Hygrothermomechanical evaluation of porous media under finite deformation. Part I – Finite element formulations 1993; 36: 147-160.
- [3] Bai M, Abousleiman Y. Thermoporoelastic coupling with application to consolidation. International Journal for Numerical and analytical methods in Geomechanics 1997; 21: 121-132.
- [4] Bathe KJ. Finite Element Procedures. Englewood Cliffs, New Jersey: Prentice-Hall, 1996.
- [5] Biot MA. Variational Lagrangian-Thermodynamics of non-isothermal finite strain mechanics of porous solids and thermomolecular Diffusion. International Journal of Solids and Structures 1977;13: 579-597.
- [6] Biot MA. The theory of propagation of elastic waves in a fluid saturated solid. J. Acoust. Soc. Am. 1956; 28: 168-191.
- [7] Borja RI, Alarcón E. A mathematical framework for finite strain elastoplastic consolidation Part 1: Balance laws, variational formulation, and linearization. Computer Methods in Applied Mechanics and Engineering 1995; 122: 145-171.
- [8] Coussy O. Thermomechanics of saturated porous solids in finite deformation. European Journal of Mechanics, A/Solids 1989; 8(1): 1-14.
- [9] Coussy O. A general theory of thermoporoelastoplasticity for saturated porous materials. Transport in Porous Media 1989; 4: 281-293.
- [10] Desai CS, Christian, JT. Constitutive laws for geologic media. In (eds), Numerical Methods in Geotechnical Engineering 1977; 73-79

- [11] Eterovic AL, Bathe KJ. A hyperelastic-based large strain-plastic constitutive formulation with combined isotropic-kinematic hardening using the logarithmic stress and strain measures. *International Journal for Numerical Methods in Engineering* 1990; 30: 1099-1114.
- [12] Kojic M, Bathe KJ. The 'effective-stress-function' algorithm for thermo-elasto-plasticity and creep. *International Journal for Numerical Methods in Engineering* 1987; 24: 1509-1532.
- [13] Lehmann T. General frame for the definition of constitutive laws for large non-isothermic elastic-plastic and elastic-visco-plastic deformations. In: T. Lehmann, ed., *The constitutive law in Thermoplasticity, CISM Courses and Lectures* 1982; 281: 379-463.
- [14] Lewis RW, Majorana CE, Schrefler BA. A coupled finite element model for the consolidation of nonisothermal elastoplastic porous media. *Transport in Porous Media* 1986; 1: 155-178.
- [15] Lubliner J. Non-isothermal generalized plasticity. In: Bui HD and Nguyeu QS ed., *Thermomechanical Couplings in Solids.*, Elsevier Science Publishers BV 1987; 121-133.
- [16] Mackinnon RJ, Carey GF. Moving-grid finite element modelling of thermal ablation and consolidation in porous media. *International Journal for Numerical Methods in Engineering* 1993; 36: 717-744.
- [17] Masters I, Pao WKS, Lewis RW. Coupling temperature to a double-porosity model of deformable porous media. *International Journal for Numerical Methods in Engineering* 2000; 49:421-438.
- [18] Pantuso D., Bathe KJ, Bouzinov, PA. A finite element procedure for the analysis of thermo-mechanical solids in contact. *Computers and Structures* 2000; 75: 551-573.

- [19] Shanghvi JY, Michaleris P. Thermo-elasto-plastic finite element analysis of quasi-state processes in Eulerian reference frames. *International Journal for Numerical Methods in Engineering* 2002; 53: 1533-1556.
- [20] Simo JC, Hughes TJR. *Computational Inelasticity*. New York: Springer-Verlag, 1998.
- [21] Simo JC, Miche C. Associative coupled thermoplasticity at finite strains: Formulation, numerical analysis and implementation. *Computer Methods in Applied Mechanics and Engineering* 1992; 98: 41-104.
- [22] Simon BR, Kaufmann MV, McAfee MA, Baldwin AL. Porohyperelastic theory and finite element models for soft tissues with application to arterial mechanics. In: Selvadural APS. (ed.), *Mechanics of Poroelastic Media* 1996, Kluwer Academic Publishers: 245-261.
- [23] Truesdell C, Noll W. Non-linear field Theories of Mechanics. In: Fluegge S. (ed.), *Handbuch der Physik* BD. III/3. Springer, Berlin 1965: 294-381.
- [24] Vardoulakis I. Dynamic thermo-poro-mechanical analysis of catastrophic landslides. *Geotechnique* 2002; 52: 157-171
- [25] Zhang H, Bai M, Abousleiman Y, Roegiers J-C. An elastoplastic analysis of non-isothermal consolidation. *International Journal for Numerical and Analytical Methods in Geomechanics* 1999; 23: 1535-1557.

Time t (before deformation)



Time $t + \Delta t$ (after deformation)

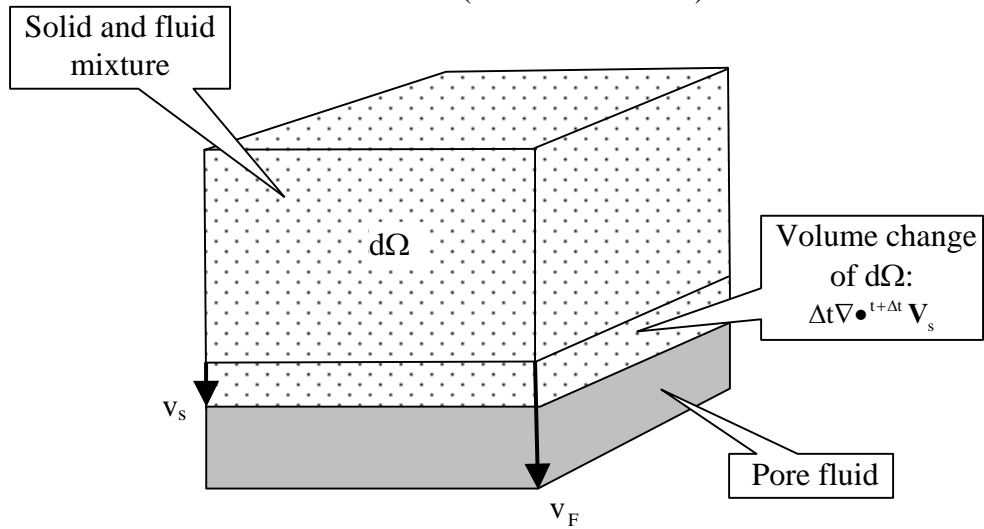


Figure 1 Mass conservation analysis for the solid-fluid mixture

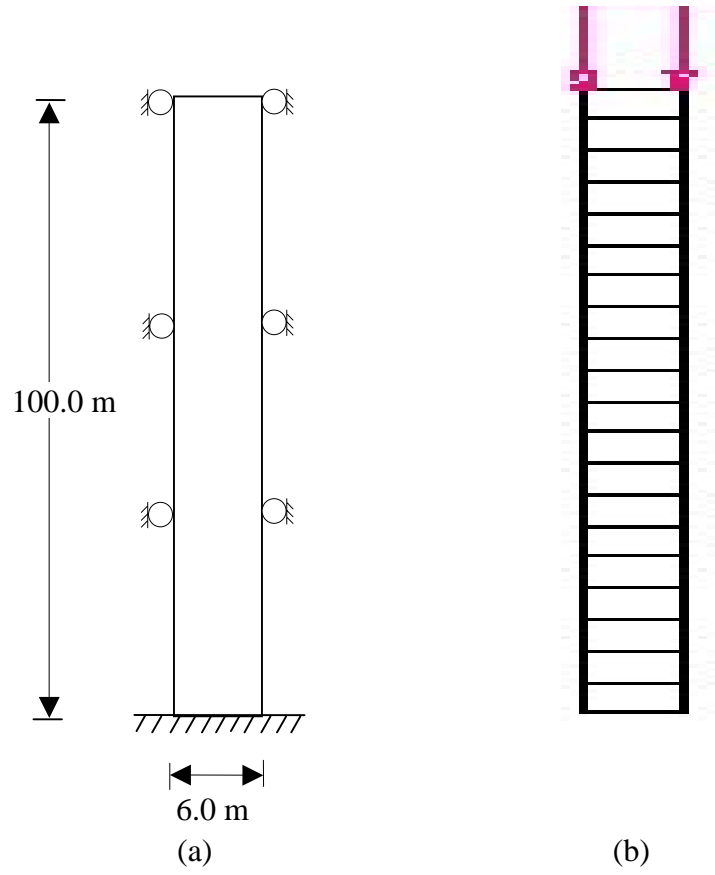


Figure 2 The scheme of the porous column and its discretization

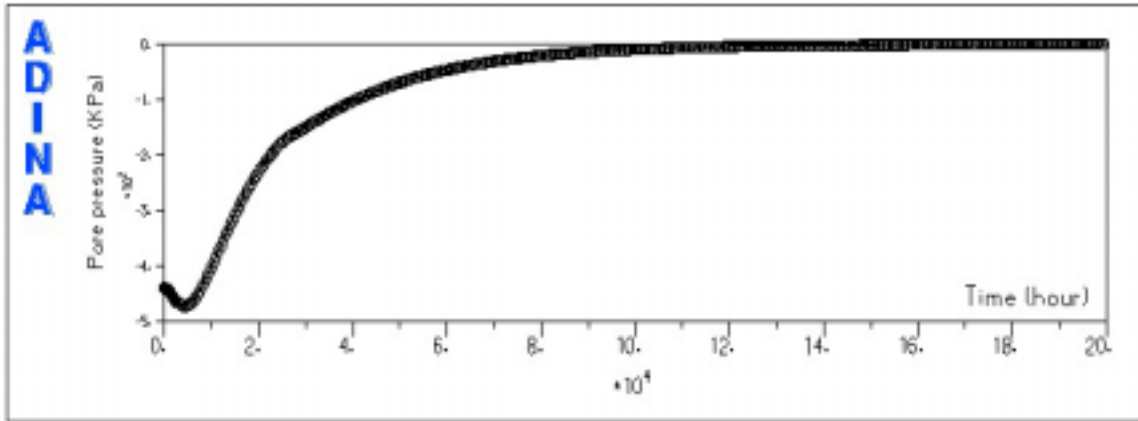


Figure 3 Dissipation of the pore pressure at the bottom of the porous column (temperature coupled)

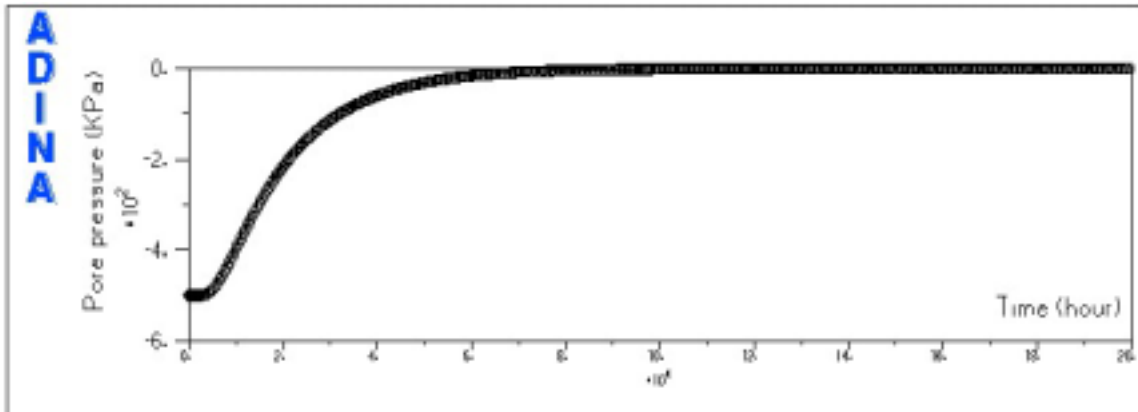


Figure 4 Dissipation of the pore pressure at the bottom of the porous column (no temperature coupled)

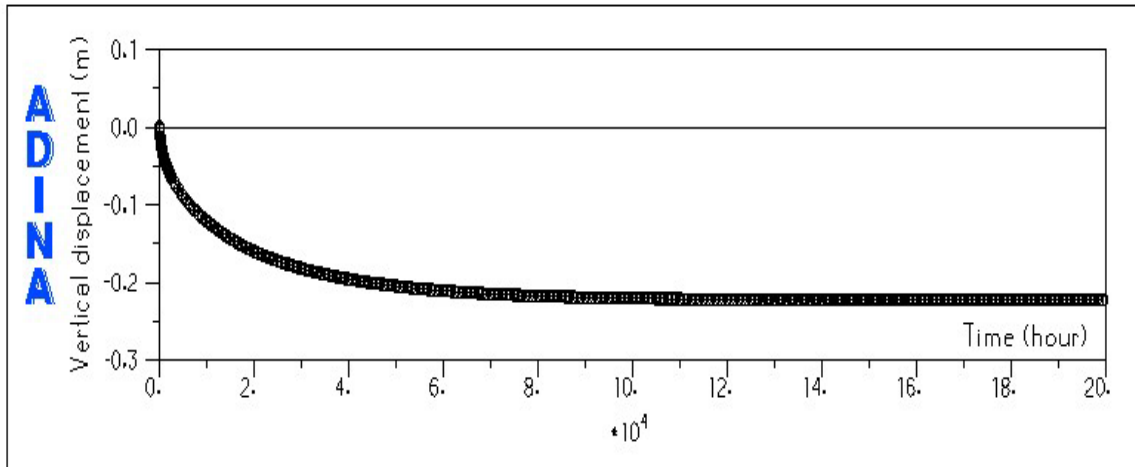


Figure 5 Vertical displacement versus time at the top of the porous column (temperature coupled)

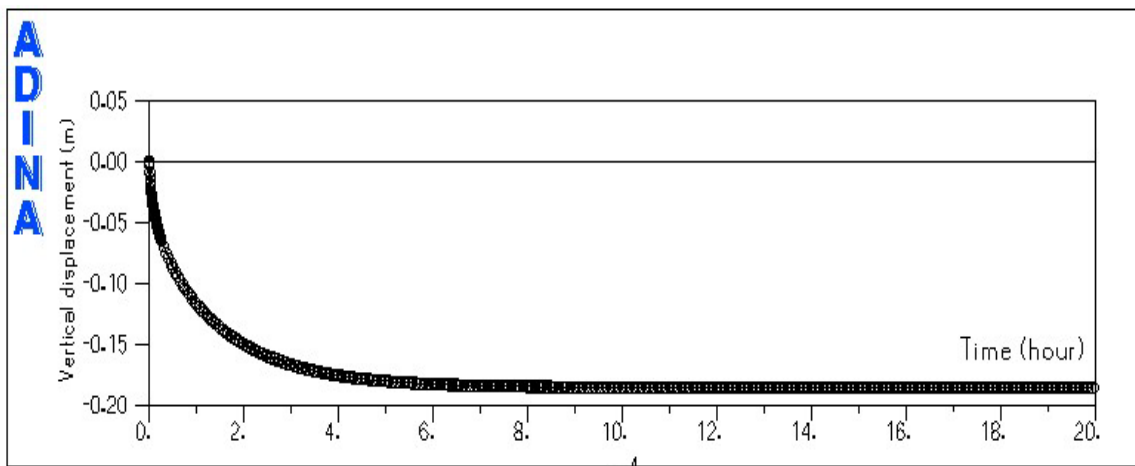


Figure 6 Vertical displacement versus time at the top of the porous column (no temperature coupled)

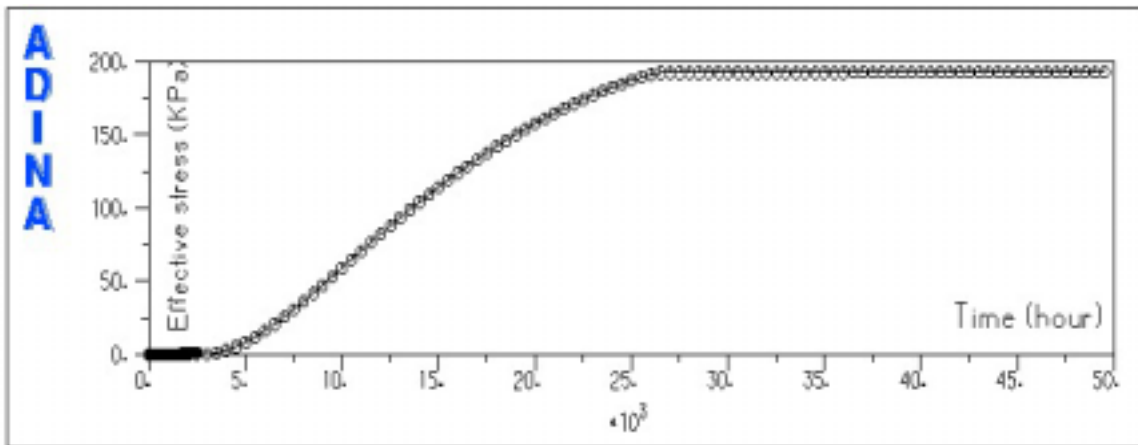


Figure 7 Changes in effective stress at the bottom of the porous column (temperature coupled)

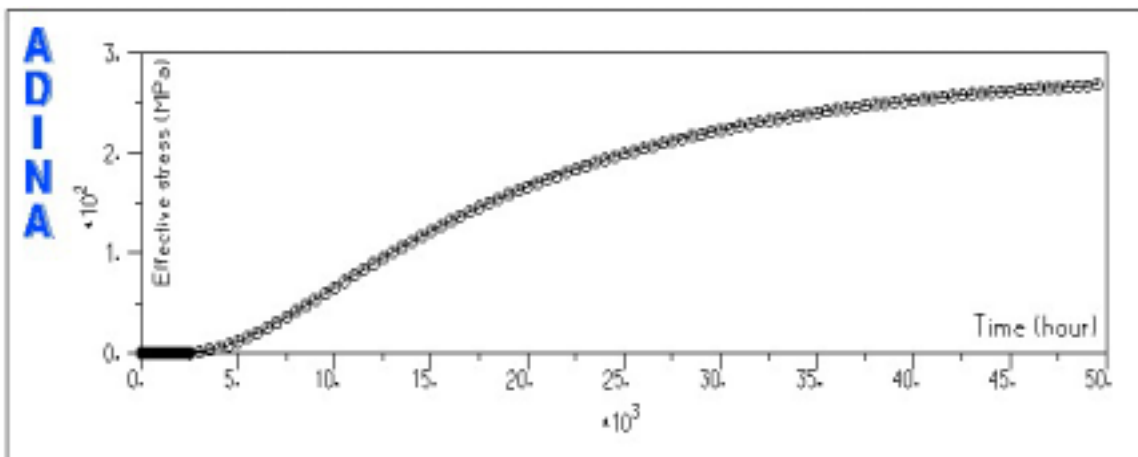


Figure 8 Changes in effective stress at the bottom of the porous column (no temperature coupled)

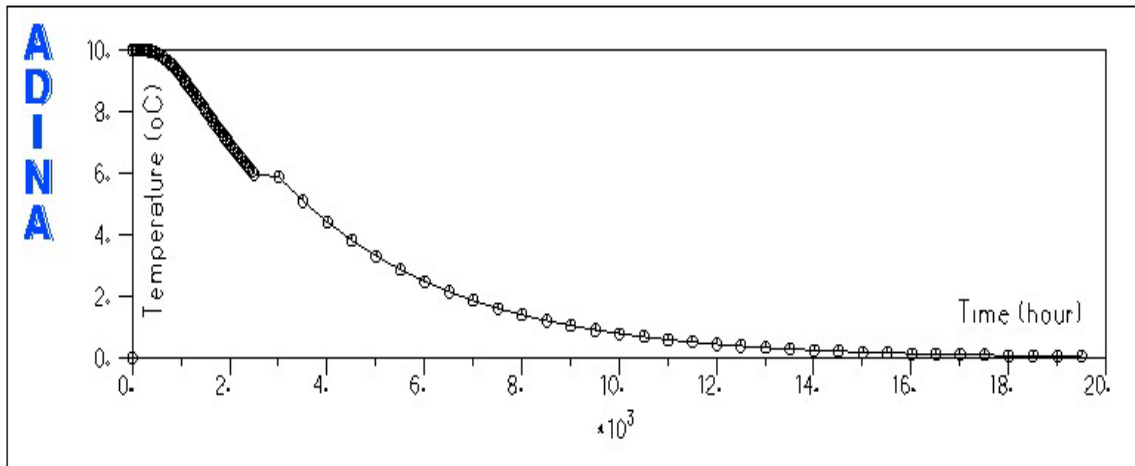


Figure 9 Temperature changes versus time at the bottom of the porous column (mechanical and thermal coupling)

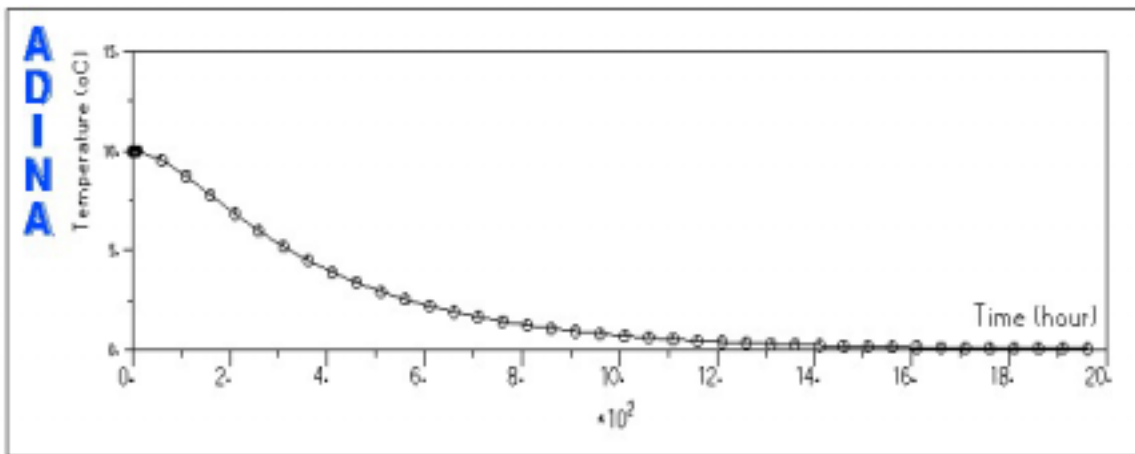


Figure 10 Temperature changes versus time at the bottom of the porous column (thermal analysis only)